Physics of Plasmas

Bifurcation-driven vertical plasma displacement

Cite as: Phys. Plasmas **29**, 054502 (2022); https://doi.org/10.1063/5.0093062
Submitted: 25 March 2022 • Accepted: 28 April 2022 • Published Online: 10 May 2022

D. I. Kiramov and B. N. Breizman

Physics of Plasmas BRIEF COMMUNICATION scitation.org/journal/php

Bifurcation-driven vertical plasma displacement

Cite as: Phys. Plasmas **29**, 054502 (2022); doi: 10.1063/5.0093062
Submitted: 25 March 2022 · Accepted: 28 April 2022 ·
Published Online: 10 May 2022

D. I. Kiramov[a] and B. N. Breizman

AFFILIATIONS

Institute for Fusion Studies, The University of Texas, Austin, Texas 78712, USA

[a]Author to whom correspondence should be addressed: Dmitrii.Kiramov@austin.utexas.edu

ABSTRACT

This paper considers vertical plasma motion resulting from plasma current decay during the disruption event. The presented filament-based model describes the motion in the ideal wall limit as an adiabatically slow evolution of the plasma equilibrium. The equilibrium exhibits a pitchfork bifurcation when the decaying plasma current passes a critical value determined by the external magnetic field. This bifurcation affects the disruption-induced mechanical loads on the first wall.

Plasma disruptions present a significant challenge for tokamaks. These events cause vertical motion of the plasma, which has been studied extensively over decades.[1–11] The vertical displacement events (VDEs) in tokamaks are related to the vertical elongation of the plasma cross section.[1] There are three different timescales involved in the VDE description: the plasma Alfvén time τ_A, the resistive wall time τ_w, and the plasma current decay time τ_p. The plasma Alfvén time is the shortest of the three. The experimental observations of the VDEs indicate (see, e.g., Refs. 3–5) that the actual timescale of the plasma motion is much longer than the Alfvén time. These observations allow one to view the VDE as an adiabatic equilibrium change rather than a rapid MHD instability. Depending on plasma and wall resistivities, the ratio of the current decay time to the resistive wall time can be large or small. This ratio distinguishes the hot VDEs from the cold VDEs. In the case of cold VDEs, we have $\tau_w/\tau_p \gg 1$, and the wall acts as an ideal conductor, confining the magnetic flux.

This work presents a simple model of the cold VDE. Some of the approximations involved are from the previous analytical[7,9,11] and numerical[12] studies. A new element of this work is the shape of the wall, which is different from the previous studies.[7,11] Our previous two-wire model of the vacuum vessel considered in Ref. 7 did not conserve the magnetic flux around the plasma, whereas the magnetic flux must stay constant on the surface of an immobile ideal wall. The model of Ref. 11 conserves the flux, but it uses two perfectly conducting plates to mimic the plasma chamber. We, herein, model the wall as a perfectly conducting cylinder, which is closer to reality and simplifies the analysis somewhat, although our conclusions are qualitatively similar to Ref. 11. We demonstrate that the plasma loses its stable equilibrium in a pitchfork bifurcation when the plasma current decays below a critical value. The initial equilibrium becomes unstable, creating two new stable equilibria. These equilibria evolve, which makes the plasma drift up or down.

We consider a plasma column confined within a perfectly conducting cylindrical wall. It is evident that the system must have a preferred direction to be vertically unstable. A corresponding anisotropy can be introduced in various ways. For example, one could consider an elongated wall.[13] In our model, we assume that the wall is circular, but an external magnetic field breaks the cylindrical symmetry. This field represents the shaping coils in a tokamak.

We model the plasma as a rigid wire that retains its cross section. This wire can move within the cylindrical chamber in a force-free way. Although a single wire does not mirror the full plasma dynamics during the VDE in all the details, it allows one to describe the vertical plasma motion qualitatively and extract some rough parametric trends to compare with the experimental and numerical data.

In Fig. 1, the plasma wire with a current $I(t)$ is located at $x = \eta(t), y = \xi(t)$, where $(\xi(t), \eta(t))$, with $\xi^2 + \eta^2 < a^2$, is the plasma displacement to be found, and a is the wall radius. The two shaping wires with a current $I_0 > 0$ are at $(0, \pm\ell)$, where $\ell > a$. We assume that at $t = 0$, the plasma current is at the geometrical center of the wall $(\xi(0), \eta(0)) = (0, 0)$. The initial position of the plasma wire must correspond to a stable equilibrium. This set-up mimics the steady state that precedes the current decay of the plasma current. The current quench starts at $t = 0$. We assume that the plasma current is a given function of time. This function can be arbitrary, as long as its timescale $\tau \sim d/dt(\ln I)$ is shorter than the resistive wall time and longer than the Alfvén time.

The magnetic field inside the wall is generated by the plasma wire, the induced wall currents, and the external conductors. We assume that the external field is stationary. In this case, the magnetic field outside the wall must be stationary. Indeed, in the ideal wall limit,

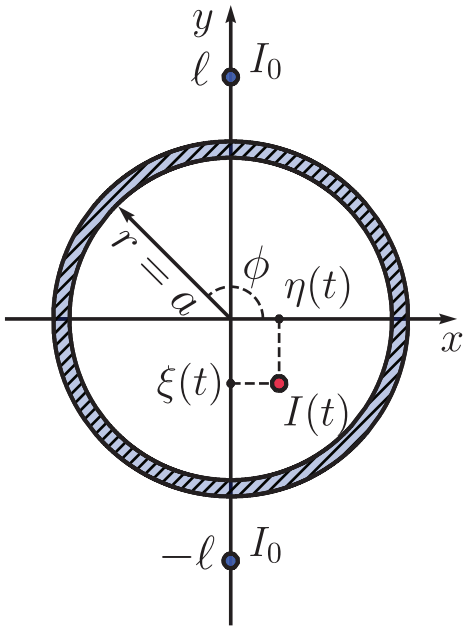

FIG. 1. A thin conducting wall of radius *a* confines a plasma rod located at $(\xi(t), \eta(t))$.

a perturbation of the magnetic field produced by the plasma current induces a surface wall current. The field of this surface current shields the exterior of the wall from the magnetic field of the plasma current.[14] In the cylindrical geometry, the field of this surface current inside the wall is equal to the field produced by a fictional image current[15,16] $I_{im} = -I(t)$ placed at $x = a^2\eta(t)/\rho^2(t), y = a^2\xi(t)/\rho^2(t)$, where $\rho^2(t) = \xi^2(t) + \eta^2(t)$. The image current and the external current exert a force on the plasma wire. We assume that the plasma column stays in a force-free state as the evolution occurs on the plasma current decay timescale. This implies that the force **F** exerted on the plasma wire vanishes for all $t \geq 0$:

$$\boldsymbol{F} = \boldsymbol{F}_{pw} + \boldsymbol{F}_{pe} = 0, \tag{1}$$

where $\boldsymbol{F}_{pe}$ and $\boldsymbol{F}_{pw}$ is the force due to the external and wall currents, respectively. Keeping in mind that the Ampère's force per unit length between two straight parallel conductors is $\boldsymbol{F}_{12} = \frac{2I_1I_2}{c^2}\frac{(\boldsymbol{r}_2-\boldsymbol{r}_1)}{|\boldsymbol{r}_2-\boldsymbol{r}_1|^2}$ in CGS units, where *c* is the speed of light, we rewrite (1) in components:

$$\begin{bmatrix} F_x \\ F_y \end{bmatrix} = -\frac{2II_0/c^2}{\eta^2 + (\ell-\xi)^2}\begin{bmatrix} \eta \\ \xi - \ell \end{bmatrix} - \frac{2II_0/c^2}{\eta^2 + (\ell+\xi)^2}\begin{bmatrix} \eta \\ \ell + \xi \end{bmatrix} - \frac{2I^2/c^2}{a^2 - \eta^2 - \xi^2}\begin{bmatrix} \eta \\ \xi \end{bmatrix} = \begin{bmatrix} 0 \\ 0 \end{bmatrix}. \tag{2}$$

The first two terms in Eq. (2) are the forces exerted by the upper and the lower external conductor, respectively (see Fig. 1). The last term is the force due to the image current.[15,16] Equation (2) determines the plasma equilibrium position in terms of the plasma current. Moreover, one can perturb the force balance (2) to analyze the linear stability of the equilibrium.

It is convenient to characterize the force **F** by an effective potential as follows:

$$\boldsymbol{F} = -\nabla U_{eff},$$

where

$$U_{eff}(\eta,\xi) = \frac{II_0}{c^2}\ln\left[\frac{\eta^2}{a^2} + \frac{(\ell-\xi)^2}{a^2}\right] + \frac{II_0}{c^2}\ln\left[\frac{\eta^2}{a^2} + \frac{(\ell+\xi)^2}{a^2}\right] - \frac{I^2}{c^2}\ln\left(1 - \frac{\eta^2}{a^2} - \frac{\xi^2}{a^2}\right). \tag{3}$$

Note that $\xi = \eta = 0$ satisfies the force balance equation (2) for any plasma current. For this equilibrium position to be stable, the effective potential Eq. (3) must have a local minimum at the origin. Evaluating the second derivatives of U_{eff} at $\xi = 0$, $\eta = 0$, we find that the origin is stable if the initial plasma current $I(0)$ is *larger* than the critical current I_c:

$$I(t=0) > 2I_0\frac{a^2}{\ell^2} \equiv I_c. \tag{4}$$

This criterion is in line with the vertical stability conditions obtained before for simplified filament-based models[16] and for realistic 2D current profiles.[17,18] Equation (4) means that the plasma current will stay at the origin as long as $I(t) > I_c$.

During the current quench phase of disruption, the plasma current decays gradually. Once the plasma current drops to the critical value I_c, the initial equilibrium bifurcates creating new equilibria. One of the equilibria is still at the origin (see the dashed line in the left panel of Fig. 2). However, this equilibrium is now unstable [see Eq. (4)]. Hence, the plasma must move to remain force-free and stable at the same time. To find the new equilibria, we solve Eq. (2) for $I(t) < I_c$. The two new solutions of (2) are given as follows:

$$\xi_\pm = \pm a\sqrt{\frac{1 - \frac{I(t)}{I_c}}{1 - \frac{I(t)}{I_c}\frac{a^2}{\ell^2}}}, \qquad \eta_\pm = 0. \tag{5}$$

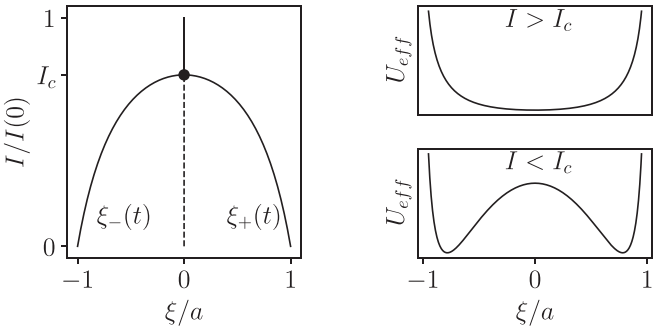

FIG. 2. Left panel: equilibrium position as a function of the plasma current. Solid and dashed curves show stable and unstable equilibria, respectively. The black dot indicates a pitchfork bifurcation. Right panels: the effective potential as a function of the vertical plasma displacement.

Evaluating the second derivatives at $\xi = \xi_\pm$, $\eta = \eta_\pm$ with respect to the plasma position of Eq. (3), we find that the new equilibria are stable if the plasma current $I(t)$ is *smaller* than the critical current I_c. As seen from Eq. (5), the plasma approaches the wall as the plasma current decays.

It is important that the presented model leaves some control options for the static phase. Indeed, one can vary the critical current I_c by changing the location of the external conductors or by adjusting their currents. In the limit of $I_0 \to 0, \ell \to \infty$, the image currents stabilize the plasma at the geometrical center. One might argue that keeping the decaying plasma current away from the wall is preferable during the uncontrolled current quench. It is then desirable to minimize the value of the plasma current at the point of contact between the drifting plasma and the first wall. On the other hand, the shaping coils create the divertor magnetic configuration and cannot simply be turned off. Hence, the external magnetic field could be optimized to keep the disruptive plasma current as low as possible at the moment of plasma–wall contact while retaining the steady-state divertor configuration within technical limits.

For $I(t) \le I_c$, the plasma vertical position is a function of the plasma current. Because of the up–down symmetry of the model, a slight jitter at the bifurcation point determines the direction of the plasma drift (see Fig. 2). Let us define the magnetic flux per unit length ψ as follows:

$$\boldsymbol{B} = \boldsymbol{e}_z \times \nabla\psi,$$

where **B** is the magnetic field and $\boldsymbol{e}_z$ is the unit vector in the direction of the z-axis (pointed out of the plot in Fig. 1). In our case, the magnetic flux inside the vacuum vessel is a superposition of the fluxes produced by individual currents: the plasma current, the image current, and the external currents. For $I(t) < I_c$, without loss of generality, we can pick one of the branches of Eq. (5) and, applying Ampère's circuital law to each current, find the total magnetic flux inside the vacuum vessel

$$\psi(r<a,\phi) = \frac{I(t)}{c}\ln\left(\frac{r^2 - 2r\xi_\pm(t)\sin(\phi) + \xi_\pm^2(t)}{a^2 - 2r\xi_\pm(t)\sin(\phi) + \frac{r^2}{a^2}\xi_\pm^2(t)}\right) + \frac{I_0}{c}\ln\left(\frac{(r^2+\ell^2)^2 - 4r^2\ell^2\sin^2(\phi)}{a^4}\right), \tag{6}$$

where we used the polar coordinate system $(r,\ \phi)$: $x = r\cos(\phi)$, $y = r\sin(\phi)$ (also see Fig. 1). The first term in (6) represents the flux of a drifting time-dependent plasma current and the flux of the image current, and the second term represents the magnetic flux of the external wires. The magnetic flux outside the ideal vacuum vessel must stay stationary,[14] thus

$$\psi(r>a,\phi) = \frac{I(0)}{c}\ln\left(\frac{r^2}{a^2}\right) + \frac{I_0}{c}\ln\left(\frac{(r^2+\ell^2)^2 - 4r^2\ell^2\sin^2(\phi)}{a^4}\right), \tag{7}$$

where the first term in (7) represents the flux of the initial plasma current, and the second term represents the magnetic flux of the external wires. Note that the magnetic flux defined by Eqs. (6) and (7) is continuous and stationary on the surface of the ideal wall[14] ($r = a$).

With Eqs. (6) and (7), we determine the surface density of the electromagnetic force acting on the vacuum vessel:[14]

$$\boldsymbol{f}(\phi) = -\frac{\boldsymbol{e}_r}{8\pi}\left[\left(\frac{\partial\psi}{\partial r}\right)^2\right]_{a-0}^{a+0} - \frac{\boldsymbol{e}_\phi}{4\pi a}\frac{\partial\psi}{\partial\phi}\left[\frac{\partial\psi}{\partial r}\right]_{a-0}^{a+0}, \tag{8}$$

where $[g]_b^a \equiv g(a) - g(b)$.

The left panel of Fig. 3 shows the contours of constant magnetic flux determined by Eqs. (6) and (7). As the plasma approaches the wall and the plasma current vanishes, the magnetic flux inside the vacuum chamber becomes predominantly determined by the external conductors. The magnetic flux does not penetrate the ideal wall, leaving the magnetic field stationary outside the vacuum vessel.

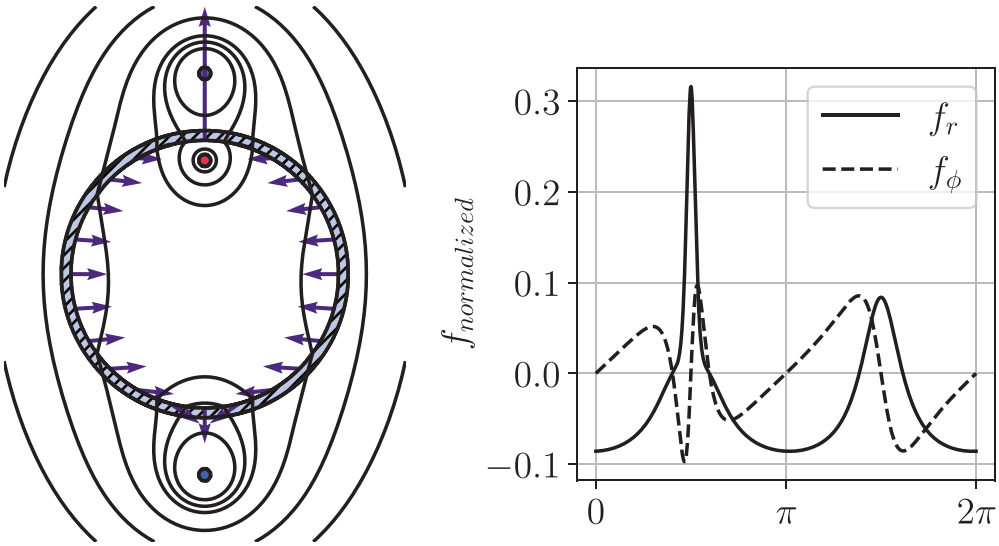

FIG. 3. Left panel: solid black curves show the contours of the poloidal magnetic flux determined by Eqs. (6) and (7); vectors represent the direction and the magnitude of the electromagnetic force surface density determined by Eq. (8). Right panel: poloidal and radial component of the normalized electromagnetic force as a function of the poloidal angle.

In the right panel of Fig. 3, we plot the normalized [$f_{normalized} = 2\pi a^2 c^2 f / I^2(0)$] surface density of the electromagnetic force [see Eq. (8)] as a function of the poloidal angle. It is noteworthy that the total force acting on the vacuum vessel vanishes in the ideal wall limit (see, e.g., Ref. 19). The local force density, on the other hand, is noticeable. The right panel of Fig. 3 shows that the radial force develops a sharp peak as the plasma approaches the first wall (see also the force distribution encoded by vectors in the left panel of Fig. 3). The peak is located near the plasma–wall contact point. In the case of a downward VDE in ITER, the peak might develop near the divertor, which can be damaging. It is, however, important to keep in mind that our simplified model of thin wire overestimates the sharpness of the peak. We also note that the poloidal currents[8,14] can modify the predicted force distribution.

The presented VDE model appears to be qualitatively consistent with the experimental observations[4] and numerical modeling.[7,10,20] To conclude, we summarize the robust trends for comparison with experiments and full-scale simulations.

We have shown that, in the ideal wall limit, the plasma with a subcritical current [see Eq. (4)] must move vertically to remain force-free. We attribute this motion to the asymmetry of the magnetic field created by the external shaping conductors. The plasma remains stable en route to the first wall, and the timescale of this motion is roughly the plasma current decay time. This adiabatic adjustment of the equilibrium position is conceptually different from the instability driven picture.[9]

This model also predicts that the initial steady-state equilibrium remains stable if the decaying plasma current is higher than the threshold value. The critical current that triggers the bifurcation [see Eq. (4)] is determined by the external conductors or the shape of the wall. Analysis of the DINA code current quench data set reveals a similar trend (see Ref. 21). It is desirable to optimize the critical current to minimize mechanical and thermal loads on the wall.

This work was supported by the U.S. Department of Energy Contract Nos. DEFG02-04ER54742 and DESC0016283.

AUTHOR DECLARATIONS

Conflict of Interest

The authors have no conflicts to disclose.

DATA AVAILABILITY

The data that support the findings of this study are available from the corresponding author upon reasonable request.

REFERENCES

[1]T. Hender, J. Wesley, J. Bialek, A. Bondeson, A. Boozer, R. Buttery, A. Garofalo, T. Goodman, R. Granetz, Y. Gribov *et al.*, "MHD stability, operational limits and disruptions," Nucl. Fusion **47**, S128 (2007).
[2]O. Gruber, K. Lackner, G. Pautasso, U. Seidel, and B. Streibl, "Vertical displacement events and halo currents," Plasma Phys. Controlled Fusion **35**, B191 (1993).
[3]G. Pautasso, D. Coster, T. Eich, J. Fuchs, O. Gruber, A. Gude, A. Herrmann, V. Igochine, C. Konz, B. Kurzan *et al.*, "Disruption studies in ASDEX upgrade in view of ITER," Plasma Phys. Controlled Fusion **51**, 124056 (2009).
[4]J. Irby, D. Gwinn, W. Beck, B. LaBombard, R. Granetz, and R. Vieira, "Alcator C-Mod design, engineering, and disruption research," Fusion Sci. Technol. **51**, 460–475 (2007).
[5]Y. Nakamura, R. Yoshino, Y. Neyatani, T. Tsunematsu, M. Azumi, N. Pomphrey, and S. Jardin, "Mechanism of vertical displacement events in JT-60U disruptive discharges," Nucl. Fusion **36**, 643 (1996).
[6]V. Riccardo, S. Walker, and P. Noll, "Parametric analysis of asymmetric vertical displacement events at jet," Plasma Phys. Controlled Fusion **42**, 29 (2000).
[7]D. Kiramov and B. Breizman, "Model of vertical plasma motion during the current quench," Phys. Plasmas **24**, 100702 (2017).
[8]D. Kiramov and B. Breizman, "Force-free motion of a cold plasma during the current quench," Phys. Plasmas **25**, 092501 (2018).
[9]D. Pfefferle and A. Bhattacharjee, "Algebraic motion of vertically displacing plasmas," Phys. Plasmas **25**, 022516 (2018).
[10]C. Clauser and S. Jardin, "ITER cold VDES in the limit of perfectly conducting walls," Phys. Plasmas **28**, 012511 (2021).
[11]A. H. Boozer, "Halo currents and vertical displacements after ITER disruptions," Phys. Plasmas **26**, 114501 (2019).
[12]R. Khayrutdinov and V. Lukash, "Studies of plasma equilibrium and transport in a tokamak fusion device with the inverse-variable technique," J. Comput. Phys. **109**, 193–201 (1993).
[13]K. Lackner, "Computation of ideal MHD equilibria," Comput. Phys. Commun. **12**, 33–44 (1976).
[14]V. Pustovitov and D. Kiramov, "Local and integral disruption forces on the tokamak wall," Plasma Phys. Controlled Fusion **60**, 045011 (2018).
[15]W. B. Smythe, *Static and Dynamic Electricity* (Hemisphere Publishing, New York, 1988), pp. 309–310.
[16]J. P. Freidberg, *Plasma Physics and Fusion Energy* (Cambridge University Press, 2008), pp. 402–405.
[17]V. Mukhovatov and V. Shafranov, "Plasma equilibrium in a tokamak," Nucl. Fusion **11**, 605 (1971).
[18]G. Laval, R. Pellat, and J. Soule, "Hydromagnetic stability of a current-carrying pinch with noncircular cross section," Phys. Fluids **17**, 835–845 (1974).
[19]V. Pustovitov, "General approach to the problem of disruption forces in tokamaks," Nucl. Fusion **55**, 113032 (2015).
[20]I. Krebs, F. Artola, C. Sovinec, S. Jardin, K. Bunkers, M. Hoelzl, and N. Ferraro, "Axisymmetric simulations of vertical displacement events in tokamaks: A benchmark of M3D-C1, NIMROD, and JOREK," Phys. Plasmas **27**, 022505 (2020).
[21]B. N. Breizman, P. Aleynikov, E. M. Hollmann, and M. Lehnen, "Physics of runaway electrons in tokamaks," Nucl. Fusion **59**, 083001 (2019).